doi:10.1016/j.jmb.2005.10.070 *J. Mol. Biol.* (2006) **355**, 282–293

JMB
Available online at www.sciencedirect.com
SCIENCE DIRECT®
ELSEVIER

Concordant Exploration of the Kinetics of RNA Folding from Global and Local Perspectives

Lisa W. Kwok[1], Inna Shcherbakova[2], Jessica S. Lamb[1], Hye Yoon Park[1] Kurt Andresen[1], Heather Smith[1], Michael Brenowitz[2,3] and Lois Pollack[1]*

[1]*School of Applied & Engineering Physics, Cornell University Ithaca NY 14853, USA*

[2]*Department of Biochemistry Albert Einstein College of Medicine, 1300 Morris Park Avenue, Bronx, NY 10461 USA*

[3]*Center for Synchrotron Biosciences, Albert Einstein College of Medicine, 1300 Morris Park Avenue, Bronx NY 10461, USA*

**Corresponding author*

Time-resolved small-angle X-ray scattering (SAXS) with millisecond time-resolution reveals two discrete phases of global compaction upon Mg^{2+}-mediated folding of the *Tetrahymena thermophila* ribozyme. Electrostatic relaxation of the RNA occurs rapidly and dominates the first phase of compaction during which the observed radius of gyration (R_g) decreases from 75 Å to 55 Å. A further decrease in R_g to 45 Å occurs in a well-defined second phase. An analysis of mutant ribozymes shows that the latter phase depends upon the formation of long-range tertiary contacts within the P4-P6 domain of the ribozyme; disruption of the three remaining long-range contacts linking the peripheral helices has no effect on the 55–45 Å compaction transition. A better understanding of the role of specific tertiary contacts in compaction was obtained by concordant time-resolved hydroxyl radical (·OH) analyses that report local changes in the solvent accessibility of the RNA backbone. Comparison of the global and local measures of folding shows that formation of a subset of native tertiary contacts (i.e. those defining the ribozyme core) can occur within a highly compact ensemble whose R_g is close to that of the fully folded ribozyme. Analyses of additional ribozyme mutants and reaction conditions establish the generality of the rapid formation of a partially collapsed state with little to no detectable tertiary structure. These studies directly link global RNA compaction with formation of tertiary structure as the molecule acquires its biologically active structure, and underscore the strong dependence on salt of both local and global measures of folding kinetics.

Keywords: RNA folding; time-resolved small-angle X-ray scattering; electrostatic relaxation; compaction; tertiary structure formation

Introduction

The addition of Mg^{2+} to the group I ribozyme from *Tetrahymena thermophila* induces folding to a biologically active conformation from an ensemble of states defined predominantly by secondary structure.[1–3] The change in the global conformation of RNA during this process can be followed by small-angle X-ray scattering (SAXS), a technique that reports on the shape, size and conformational distribution of macromolecules.[4] Time-resolved SAXS studies, conducted using a continuous-flow mixer, access global structural changes with millisecond time-resolution.[5] SAXS analysis of the *T. thermophila* L-21 Sca1 ribozyme has shown that when Mg^{2+}-mediated folding is initiated from a low ionic strength condition, the RNA ″relaxes″ from an extended and rigid to a flexible and more compact ensemble of conformations; a second, slower transition is linked to the formation of five long-range tertiary contacts.[5,6] These long-range tertiary contacts are depicted in Figure 1. Prior studies monitoring local structure formation during Mg^{2+}-mediated folding of the *Tetrahymena* ribozyme revealed a hierarchy of rates in the formation of the native tertiary structure of P4-P6 domain > periphery > catalytic core.[7,8]

The present studies further explore the relationship between compaction and the formation of discrete tertiary interactions during RNA folding utilizing concordant measures of changes in global conformation and local tertiary structure. Hydroxyl radical

---

Abbreviations used: SAXS, small-angle X-ray scattering.

E-mail address of the corresponding author: lp26@cornell.edu

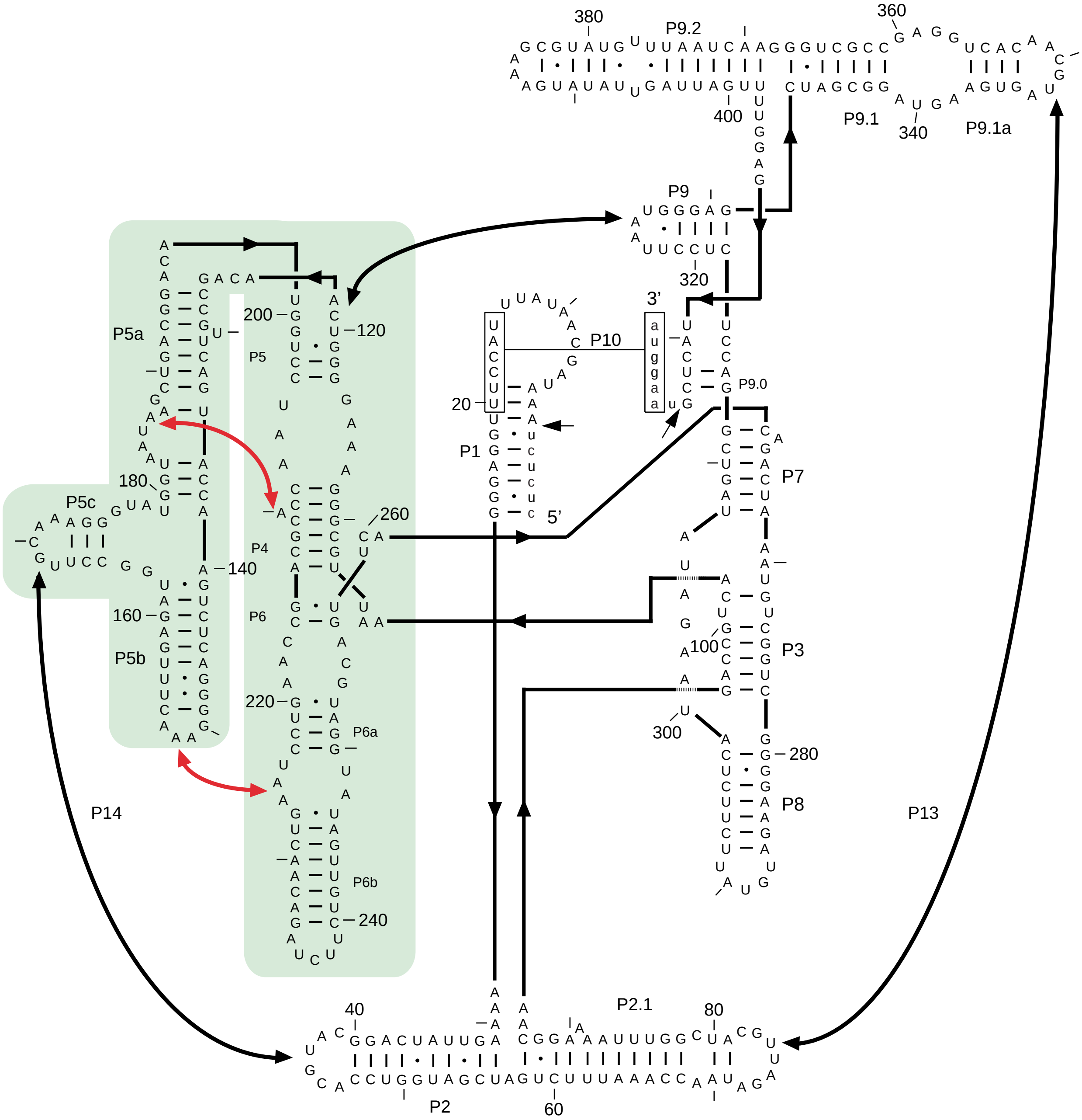

Figure 1. A representation of the secondary and tertiary structure of the *Tetrahymena* Sca L-21 ribozyme with the P4-P6 domain highlighted in green. The five long-range tertiary contacts are indicated with curved arrows. The two contacts within P4-P6 are indicated with red arrows, the three peripheral contacts are indicated with black arrows.

(·OH) footprinting is a well-established measure of changes in the solvent accessibility of the phosphodiester backbone of RNA with resolution as fine as a single nucleotide.[9,10] Synchrotron X-ray ·OH footprinting reports the time-evolution of discrete tertiary contacts also on the millisecond timescale.[11,12] Matched SAXS and ·OH footprinting analysis of wild-type ribozyme and judiciously selected mutants provide a definitive exploration of the kinetics of global compaction and tertiary contact formation during the Mg^{2+}-mediated folding of RNA.

Since the P4-P6 domain is the first to fold upon the addition of Mg^{2+} from a very low salt initial condition,[8] it is natural to question its role in the compaction kinetics. Experiments that probe the role of contacts within or exterior to the P4-P6 domain are thus a focus of our investigations. The data provide compelling evidence that: (i) the majority of tertiary contact formation occurs within a relaxed, screened, and moderately compact ensemble of molecules; (ii) the compaction due to tertiary contact formation depends on folding of the P4-P6 domain; and (iii) the reorganization of the misfolded catalytic core occurs within a highly constrained conformational space with either minor or no further compaction. The generality of these results and the importance of ambient ionic strength in cation-mediated RNA folding will be discussed.

Results

Time-dependent global compaction

Global compaction of the ribozyme is assessed by calculating the molecule's time-dependent radius of gyration, R_g, from the angular dependence of X-rays scattered to the lowest angles. In the first set of studies, wild-type ribozyme and three mutants deficient in combinations of internal P4-P6 and peripheral tertiary contacts (Figure 1) were folded from an initial condition of 50 mM Mops (pH 7) by the addition of Mg^{2+} to a final concentration of 10 mM. The R_g of the wild-type ribozyme decreases from 75 Å to 55 Å within the first 10 ms of the folding reaction. A second compaction transition occurs within 100 ms, further reducing R_g to 45($\pm$1) Å, comparable to that of the fully folded molecule (Figure 2(a)).[13]

The "quintuple" mutant, deficient in both the internal P4-P6 and periphery long-range contacts, shows only the fast kinetic phase with R_g decreasing from 75 Å to 57 Å (Figure 2(a)). This result is consistent with previous studies analyzed by projecting each time-dependent scattering profile onto a linear combination of unfolded and folded states.[6] A finer dissection of the role of tertiary contacts in mediating compaction was undertaken by measuring the folding of the "double" mutant lacking only the two internal P4-P6 contacts and the "triple" mutant lacking the three peripheral contacts (Figure 2(b)). The double mutant displays only a single, fast kinetic phase, analogous to the kinetic folding profile measured for the quintuple mutant. Folding of the triple mutant closely parallels that of the wild-type: following the fast kinetic phase is the second compaction transition to $R_g = 44$ Å.

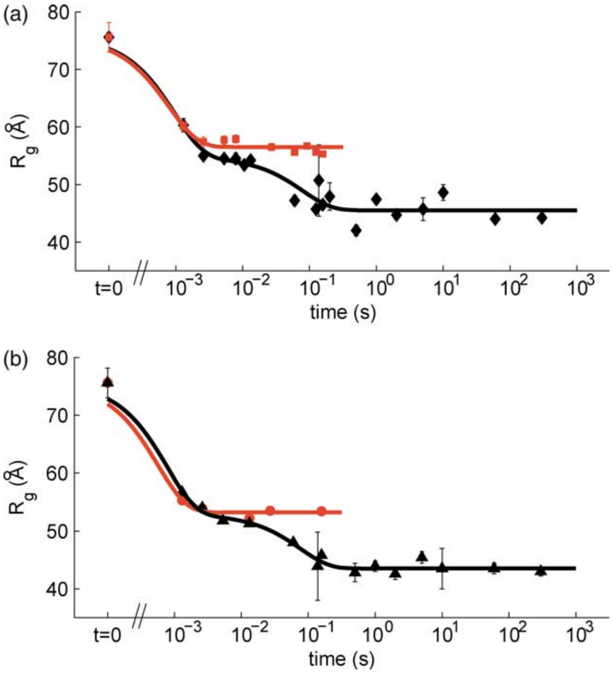

Figure 2. Time-dependent radius of gyration (R_g) measured during Mg^{2+}-mediated folding of wild-type L-21 ribozyme and selected mutants. Folding was initiated from 50 mM Na–Mops buffer (20 mM Na^+) by the addition of $MgCl_2$ to a final concentration of 10 mM Mg^{2+}. (a) R_g of wild-type ribozyme (black diamonds) and the quintuple knockout mutant (red squares) in which all five long-range contacts of Figure 1 have been destabilized by sequence mutation. Compaction of the wild-type ribozyme occurs in two phases: within 10 ms, R_g decreases from 75 Å to 55 Å, a second compaction to 45 Å follows within 100 ms. In contrast, the quintuple mutant displays only a single, rapid compaction from 75 Å to 57 Å. (b) R_g of the "double knockout mutant" (red circles) with the two P4-P6 domain internal contacts destabilized and the "triple knockout mutant" (black triangles) with three destabilized peripheral contacts. Compaction of the double mutant occurs in a single rapid phase, reminiscent of the quintuple mutant, while compaction of the triple mutant occurs in two phases, analogous to the wild-type ribozyme.

The data present a consistent picture of the global changes that accompany folding. The earliest observable event in Mg^{2+}-mediated folding is a significant rapid compaction. This rapid compaction is observed for both the wild-type and mutant RNA molecules lacking long-range tertiary contacts. The second transition occurs only in RNA molecules that support the formation of the P4-P6 domain. At the end of the second kinetic phase, the molecular radius of gyration is close to native. Thus, formation or rearrangements of tertiary interactions slower than those causing the P4-P6 domain to fold do so within a compact envelope and without a "signature" easily measured by SAXS. We therefore turned to ·OH footprinting to link molecular compaction directly with the formation of individual tertiary contacts.

Time-dependent formation of tertiary contacts

Time-resolved ·OH footprinting studies were carried out to monitor directly local changes in the solvent accessibility of the RNA backbone during folding and to relate them to global compaction. Because the 50 mM Mops present here and in published SAXS studies[5,6] is a potent scavenger of ·OH, its presence in the footprinting buffer would increase the required X-ray exposure and thus lengthen the minimal accessible times. Since our focus is on the earliest folding events, we first sought to match the footprinting to the SAXS experiments by substituting sodium cacodylate buffer (which does not scavenge ·OH) for Mops and matching the total ionic strengths of the solution (see Materials and Methods).

Figure 3 shows progress curves for ·OH protections representative of the three major regions of the ribozyme: the P4-P6 domain, the catalytic core and the periphery obtained under these experimental

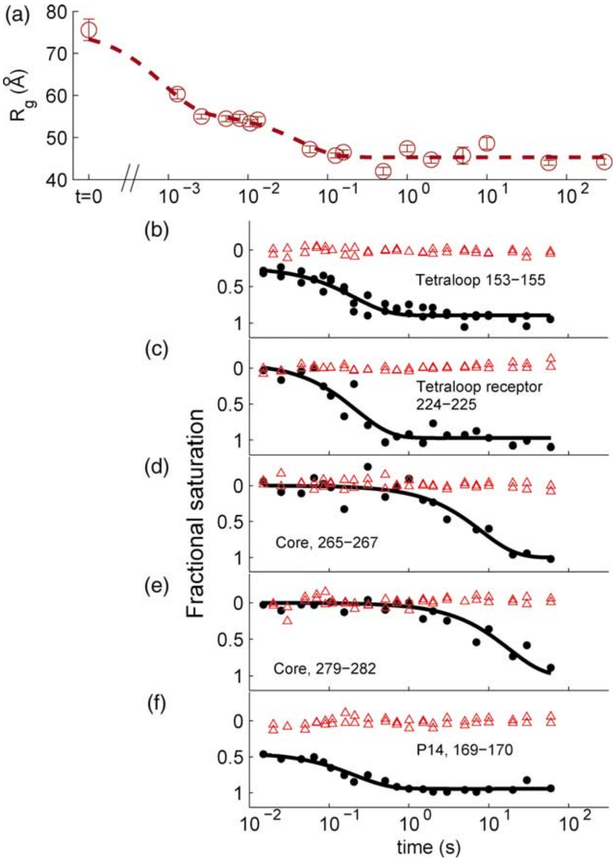

Figure 3. Hydroxyl radical (·OH) protection data from the three main regions of the ribozyme, P4-P6 domain, core and periphery, under solution conditions similar to those reported in the legend to Figure 2. (a) The time-course of R_g of wild-type L-21 ribozyme from Figure 2(a) is shown for comparison. (b) and (c) Kinetic progress curves monitoring protection of residues within the P4-P6 domain indicate that it forms early in the wild-type molecule (filled black circles): fractional saturation of both (b) the L5b tetraloop (residues 153–155) and (c) the tetraloop receptor (residues 224–225) are shown, along with best fit (equations used to determine the rate constants are given in the text). The L5b tetraloop progress curve is best fit with a 19% burst amplitude. Protection of regions within the catalytic core ((d) residues 265–267; (e) residues 279–282) occur an order of magnitude more slowly than in P4-P6. (f) The kinetic progress curve for one half of the P14 long-range contact (residues 169–170) includes a 40% burst amplitude with additional protection occurring on a time-scale similar to that measured for P4-P6. Protections of these regions within the double knockout mutant, with destabilization of P4-P6 internal contacts, are shown as open triangles in (b)–(f). No change in protection is measured relative to the initial state at any position.

conditions. Each ·OH progress curve is a transition that is scaled from the extent of ·OH cleavage present in the initial buffer (fractional saturation, $\bar{Y}=0.0$) to that measured for a folded control equilibrated in 10 mM Mg^{2+} ($\bar{Y}=1.0$). The majority of measured ·OH progress curves are described well by a single exponential spanning the full range of $\bar{Y}$ from 0.0 to 1.0. In contrast, other sampled ·OH protections, e.g. P14 and the L5b tetraloop, display burst amplitudes within which changes in solvent accessibility occur faster than can be sampled by the present time-resolved footprinting assay (Figure 3(b) and (f)).

We consider in turn the formation of the three distinct regions that delineate the low-salt folding kinetics: the P4-P6 domain, the core and periphery.[8] Since the SAXS profiles link contacts within P4-P6 to the 55–45 Å compaction (Figure 2), it is natural to compare in detail the time-scale of P4-P6 domain formation to global compaction. Formation of the L5b tetraloop–tetraloop receptor interaction was followed as a measure of closure of the P4-P6 domain into its native folded structure. The kinetic progress curve for the tetraloop receptor (nucleotides 224–225) is described by a single exponential with a rate of 4.7 (-1.6, $+2.0$) s^{-1} (Figure 3(c)). While this ·OH protection displays no burst amplitude, its partner tetraloop does. Protection of the L5b tetraloop is best fit with a burst amplitude of 19% followed by a transition with a comparable rate of 4.5 (-1.8, $+2.7$) s^{-1} (Figure 3(b)). Such a dichotomy between the two sides of a tertiary contact has been interpreted to reflect formation of a non-native tertiary interaction by the divergent partner.[14] From these data, we conclude that closure of the P4-P6 domain hairpin-like structure occurs at a rate of 4.5–4.7 s^{-1} under these experimental conditions.

The prior observation that the P4-P6 domain folds more rapidly than the catalytic core[8] holds true under these experimental conditions, although the ionic strength is slightly higher here (~20 mM *versus* ~8 mM M^{+}) and the temperature lower (25 °C *versus* 42 °C). The changes in local solvent accessibility associated with folding of P4-P6 are shown in Figure 3(b) and (c), catalytic core protections are shown in Figure 3(d) and (e). The progress curves show core protections form an order of magnitude more slowly than the other regions of the ribozyme, and are described well by a single exponential spanning the full range of fractional saturation. Thus, formation of the native tertiary contacts that define the catalytic core occurs entirely within the compact ensemble constrained by the folding of the P4-P6 domain.

In contrast to the retention of the relative folding rates of the P4-P6 domain and the catalytic core, ~40% of the L5c side of the P14 long-range peripheral contact forms within the 15 ms dead-time of the footprinting experiments, while the time-dependence of the remainder of the reaction amplitude is coincident with the P4-P6 domain (Figure 3(f)). This result differs from the previously observed lag in formation of the periphery relative to the P4-P6 domain and highlights the substantial changes that can result from even subtle differences in experimental conditions. Since folding of P4-P6 as well as structuring of P5abc is required for formation of the P14 contact, the burst amplitude of this ·OH protection progress curve likely represents rapid formation of a non-native interaction, as concluded for the L5b tetraloop ·OH protection. For ·OH protections with burst amplitudes, such as the L5b tetraloop and P14 (Figure 3(b) and (f)), their initiation during the first SAXS transition cannot be ruled out (Figure 2).

To further explore the link between P4-P6 domain formation and compaction, ·OH protections of the double mutant RNA, lacking the two tertiary contacts that stabilize the P4-P6 domain, were measured. The initial collapse of this construct reported by SAXS occurs within the dead-time of the footprinting experiments; no further compaction of the ″double mutant″ ribozyme was observed by SAXS on timescales longer than 10 ms (Figure 2(b)). The corresponding synchrotron footprinting progress curves likewise show no change over the timescale analyzed; increases in $\bar{Y}$ from zero were not observed for any ·OH protection analyzed (Figure 3(b)–(f)). Thus, the local measures of solvent accessibility of all regions remain unchanged after initiation of the folding reaction. SAXS and footprinting agree that formation of the stable tertiary structure is dependent upon formation of the ″clamped″ hairpin-like structure of the P4-P6 domain that is absent from the double mutant RNA. This result is consistent with the role of the P4-P6 domain as a folding scaffold, and supports the conclusion that the fast compaction measured by SAXS is predominantly an electrostatic relaxation and proceeds without formation of stable tertiary contacts. This conclusion will now be considered with regard to the ·OH footprinting progress curves obtained for the wild-type ribozyme.

The measured footprinting curves for the wild-type and double mutant ribozymes are consistent with the conclusion that folding of the P4-P6 domain dominates the second compaction transition measured by SAXS. Since footprinting and SAXS report different molecular properties, direct comparison of these data is dependent upon the method used to relate these two measures of folding quantitatively. The data were matched by scaling the change in R_g that occurs during this compaction to the change in ·OH protection measured over the same timescale to focus on the local events that underlie the second global compaction. This juxtaposition was accomplished by aligning the first measurable time-point of the ·OH footprinting progress curve (15–20 ms) with the corresponding value of R_g from the SAXS curve and the plateaus achieved by both progress curves about 1 s following the initiation of folding. Although a direct comparison of time constants would be useful, there is a large error bar on some of the SAXS-derived time constants due to the limited number of data points acquired.

The alignment of the SAXS profile with that of the L5b tetraloop and L5b tetraloop-receptor ·OH protection progress curve is shown in Figure 4. These two transitions match up closely, but not exactly; the SAXS transition is consistently faster than those determined by ·OH footprinting. To test whether this differential is the result of a small mismatch in the solution conditions used for the two techniques, a new set of experiments was conducted at solution conditions different from those utilized in SAXS analysis of the *Tetrahymena* ribozyme.

Precise matching of the initial folding conditions

The different experimental requirements of ·OH footprinting relative to SAXS resulted in small variations of the buffer solutions used in the studies described above. Since folding of the *Tetrahymena* ribozyme is highly sensitive to the ionic conditions, especially at low ionic strength, small differences in monovalent ion concentration can yield dramatic changes in the folding kinetics.[10,14–16] Thus, we designed and carried out additional SAXS and ·OH footprinting measurements in a solution with higher, precisely matched total monovalent ion concentration.

The increase in the background ionic strength during Mg^{2+}-mediated folding has several effects on molecular compaction (Figure 5). As expected, the ribozyme in its initial state at 100 mM KCl appears to be partially compact,[17] displaying

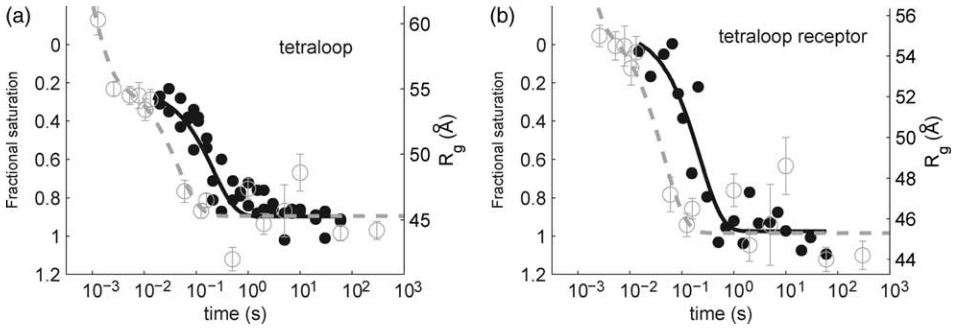

Figure 4. Comparison of footprinting protection kinetics (black lines and filled symbols) with compaction kinetics (gray dotted lines and open circles) for (a) the L5b tetraloop and (b) the tetraloop receptor. Formation of the P4-P6 domain, assayed by contact between these partners, appears delayed relative to the 55–45 Å compaction reported by SAXS, under these solution conditions (20 mM M^+).

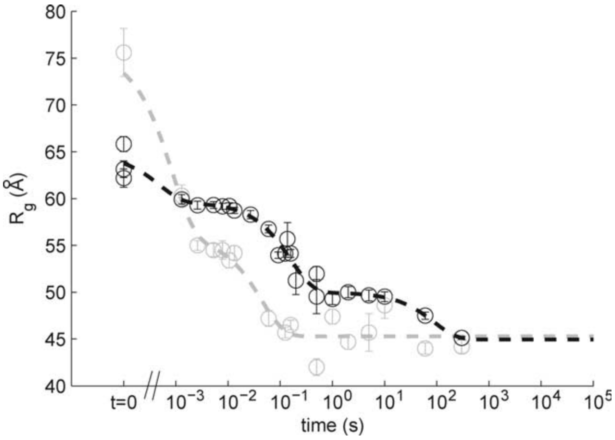

Figure 5. Compaction kinetics of the wild-type L-21 Sca I ribozyme at higher background monovalent ionic strength (100 *versus* 20 mM M^+) upon folding induced by the addition of 10 mM Mg^{2+}. Progress curves at lower background ionic strength (light gray line and circles) are superimposed for comparison of initial R_g values (64 Å at higher salt *versus* 75 Å at lower salt, due to additional screening of the phosphate backbone as the monovalent concentration is increased) and R_g values at the end of the rapid compaction (60 Å at higher salt, as opposed to 55 Å at lower salt, see the text). The amplitude and rate constant of the second compaction are similar at the different background salt concentrations. A third kinetic phase, present only at higher salt, brings the R_g of the ribozyme to its native value.

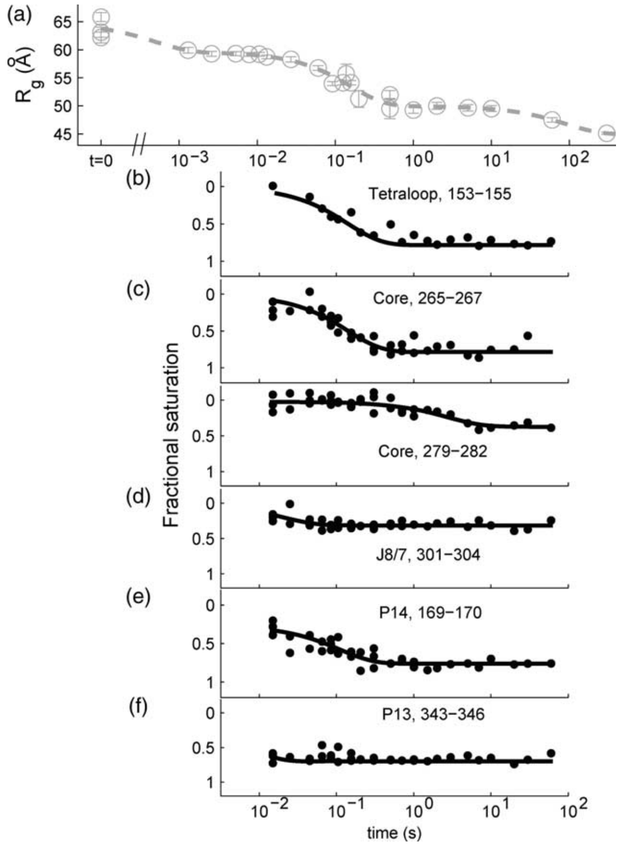

Figure 6. Hydroxyl radical (·OH) protection data from the three main regions of the wild-type ribozyme, P4-P6 domain, core and periphery, under the higher ionic strength solution conditions reported in the legend to Figure 5. (a) The time-course of R_g of wild-type L-21 ribozyme from Figure 5 is shown for comparison. (b) Kinetic progress curves within the P4-P6 domain indicate that it forms early (filled circles). In contrast to the lower salt measurements, no burst phase amplitude is measured for the L5b tetraloop (153–155). Core protections are shown in (c)–(e). Some residues within the core, e.g. 265–267, acquire protection from hydroxyl radicals coincidently with the P4-P6 domain under these conditions, while other parts of the core form more slowly. Formation of the peripheral contacts is also heterogeneous at higher ionic strength, with some protections occurring within the dead-time of the footprinting assay ((g), residues 343–346) or coincidently with P4-P6 folding ((f), residues 169–170).

a smaller R_g, due to phosphate backbone screening at the higher ambient concentration of monovalent cation. Upon the initiation of folding, R_g decreases to 60 Å at the end of the first phase of compaction, compared with 55 Å measured at the same time in the lower-salt transitions. The amplitudes and rate constants of the second phase of the compaction are comparable for both experimental conditions. A third kinetic phase, present at the elevated concentration of monovalent cations, occurs on a timescale of tens to hundreds of seconds and brings the ribozyme compaction to its native state with $R_g = 45$ Å.

The ·OH protection progress curves that were obtained under these new experimental conditions (Figure 6), are significantly different from those acquired at lower ionic strength (Figure 3). A near or exact coincidence of structure formation reported by footprinting, and compaction reported by SAXS is observed throughout the molecule. Indeed, the progress curve determined for the L5b tetraloop (nucleotides 153–155), that reports completion of the folding of the P4-P6 domain, coincides exactly with the second phase of global compaction progress curve (Figure 7(a)) when the two data sets are aligned as in Figure 4. A striking difference in folding under these experimental conditions is the heterogeneous organization of the catalytic core; core ·OH protection 265–267 (Figure 6(c)) forms coincidently with the L5b tetraloop and the second phase of global compaction (Figure 7(b)). Furthermore, the ·OH protection for the long-range peripheral contact P14 (Figure 6(f)) forms at about the same rate as (or slightly faster than) the second global compaction phase (Figure 7(c)). From these results, we conclude that the slight delay in the formation of tertiary structure of the P4-P6 domain in comparison to the second phase of global compaction observed at low ionic strength reflects a slight mismatch of the ionic conditions of the experiments; tertiary contact formation and

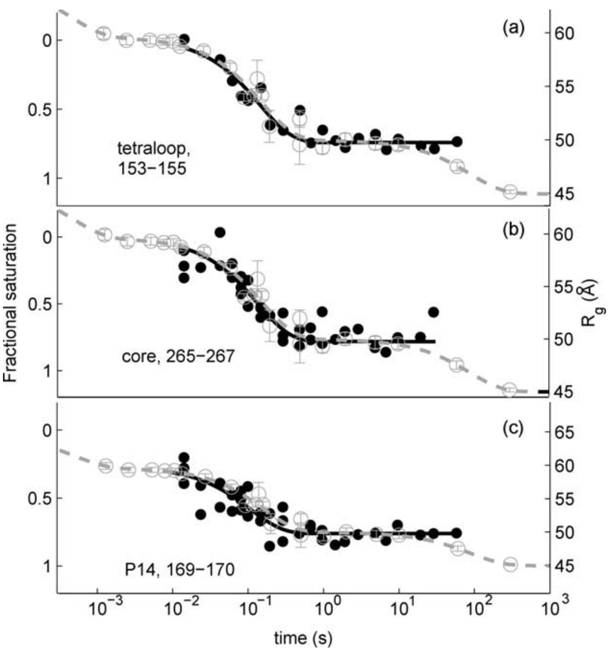

Figure 7. Comparison of footprinting protection kinetics (black lines and filled symbols) with compaction kinetics (gray dotted lines and open circles) at higher background monovalent salt. Protections coincident with the second SAXS compaction occur in all regions of the ribozyme: in P4-P6 ((a) residues 153–155), in the core ((b), residues 265–267) and in the periphery ((c), residues 169–170).

the second global compaction transition occur coincidently. Overall, a greater range of tertiary contacts is coincident with the second compaction transition in this second experimental condition. However, since comparable changes in R_g are measured at the low-salt and high-salt folding conditions (Figures 2(a) and 5), this observation strengthens the view that folding of the P4-P6 domain dominates this compaction.

The strong dependence of Mg^{2+}-mediated ribozyme folding on the concentration of monovalent cations present is highlighted by examining the order of formation of different regions of the ribozyme. In contrast to the core's folding behavior observed at low salt, the structuring of the catalytic core is not a homogenously slow process (I.S and M.B., unpublished results, and this work).[8,14] As noted above, the ·OH protection for nucleotides 265–267 forms coincidently with the P4-P6 domain (Figure 7(a) and (b)). In contrast, the observable transitions of nucleotides 279–282 (Figure 6(d)) and 301–304 (Figure 6(e)) occur completely within the 50 Å intermediate. A significant portion of the reaction amplitude of both ·OH protections remains after 60 s, the longest time-point sampled; it is not clear from these data whether these reactions continue through the slowest SAXS transition or remain partially folded for longer times.

Formation of the long-range peripheral contacts is also not a homogeneous process under these experimental conditions. As noted above, the ·OH protection for P14 forms nearly coincidently with the P4-P6 domain (Figure 7(c)) in contrast to the long-range contact P13 that is almost completely formed within the dead-time of the footprinting assay (Figure 6(g)). Organization of the periphery begins prior to folding of the P4-P6 domain. Since the minimum time accessible to the footprinting assay (15 ms) is longer than that for SAXS (1 ms), participation of this contact in the initial phase of global compaction cannot be excluded.

Some of the ·OH protections plateau at values of $\bar{Y} < 1.0$, indicating the presence of very slow folding transitions. Such slow processes are not unusual in cation-mediated folding reactions of large RNA molecules at lower temperatures; these processes typically reflect resolution of misfolded species. Since the focus of this study is on the earliest folding events, longer reaction times and hand-mixing experiments capable of fully resolving these slow transitions were not conducted.[14] In this case, resolution of the misfolded molecules is accompanied by further compaction (Figure 5).

Discussion

This study presents an exceptional view of early events during the Mg^{2+}-mediated folding of the *Tetrahymena* ribozyme from both global and local perspectives. The course of the SAXS progress curves following global compaction depend upon long-range tertiary contacts within the ribozyme as well as on ionic conditions of the folding reaction. One, two or three kinetic phases are present depending upon these variables. Time-resolved ·OH footprinting was used to follow the local changes in solvent accessibility that underlie these global transitions. Application of these complementary approaches reveals that the relationship between global compaction and the formation of stable tertiary contact formation changes over the course of the folding reaction.

The earliest compaction transition is observed in all the ribozyme constructs; the resultant first intermediate appears to be predominantly, but not purely relaxed; small amounts of non-native (and possibly native) tertiary contacts may be present within it, depending on solution conditions. Further compaction of the first intermediate proceeds through a second transition that clearly depends upon the formation of stable tertiary interactions. Following this latter compaction, the radius of gyration is close to that of the native folded ribozyme, within which additional tertiary interactions are observed to form. The division of the folding events into compaction without tertiary contact formation, compaction with tertiary contact formation and tertiary contact formation without compaction is justified and is further explored below.

A rapid, initial compaction is observed in the SAXS progress curves obtained for the wild-type ribozyme and the mutants in which combinations of long-range contacts were disabled by mutation. A precise time constant was not obtained, since most of this compaction transition occurs prior to the first sampling at 1 ms. In the low-salt background, the wild-type and long-range mutant RNA molecules are all characterized by $R_g \cong 75$ Å in the absence of Mg^{2+}, showing that the long-range contacts do not influence the global conformation of the initial state significantly. Since the size of the first compact intermediate depends only weakly on the presence of long-range contacts (Figure 2), we conclude that the first intermediate is mostly devoid of stable tertiary structure. This conclusion is supported by the absence of any local changes in solvent accessibility upon the addition of Mg^{2+} to the double mutant ribozyme (Figure 3).

However, the presence of burst amplitudes in several ·OH protection progress curves suggests that at least a small measure of tertiary contact formation occurs early in folding (Figure 3(b) and (f); L5b tetraloop and P14, respectively). It is not possible to assign rate constants to these early protections due to the limited time-resolution of footprinting experiments compared with SAXS. Hence, we cannot discern whether a burst phase in the ·OH footprinting progress curves occurs in concert with the rapid compaction measured by SAXS. Since a burst amplitude is not evident in the tetraloop receptor ·OH progress curve, we believe that the burst amplitude of the L5b tetraloop reflects formation of a non-native interaction. A similar conclusion is drawn for the P14 ·OH protection, 169–170; structuring of this region into the conformation suitable for formation of the long-range contact does not occur until after the P4-P6 domain folds.[18]

The presence of non-native contacts in the first intermediate is supported also by the different values of R_g obtained under the two folding conditions for the wild-type and mutant RNA molecules studied. However, these differences alone are insufficient to elucidate the nature of the non-native contacts. They could stabilize either a more extended or more compact structure. Since ·OH footprinting cannot identify the partners involved in the hypothesized misfolds, little can be said about the structure of the earliest intermediates. In spite of the small differences between R_g values measured at the two experimental conditions, the non-specific character of the fast SAXS compaction transition is ubiquitous. This conclusion confirms the previous suggestion linking this compaction to an electrostatic relaxation of the helices following the screening of the negative charge of RNA by the added cations.[6] At these early reaction times, however, this process may include formation of some native and non-native tertiary interactions that are few in number, and result in R_g changes that are a fraction of the overall compaction. Thus, rapid compaction accompanied by minimal structure formation implies that the majority of tertiary contact formation occurs subsequently, from within a compact ensemble of structures.

The second global compaction transition is present only in ribozyme molecules within which folding of the P4-P6 domain occurs. Both the wild-type and triple mutant ribozymes support P4-P6 formation, unlike the quintuple and double mutants (Figure 2). While the SAXS profiles alone show the necessity of P4-P6 formation to the second compaction, the ·OH footprinting results obtained for the double mutant further accentuate the importance of the P4-P6 domain to ribozyme folding; in the absence of P4-P6 stable tertiary interactions cannot form anywhere in the ribozyme (Figure 3 and data not shown). Even the burst phase protections vanish during folding of the double mutant, suggesting that the local structure of the L5c loop is affected by the mutations that weaken the interhelix interactions stabilizing P4-P6.

The absence of detectable tertiary structure in the double mutant ribozyme may seem perplexing, given the native-like protections observed for the Δ P5abc ribozyme, a construct in which the P5abc element has been removed.[19] While the P4-P6 domain cannot form in the absence of P5abc, folding of the Δ P5abc ribozyme occurs, albeit at higher concentrations of magnesium than we used in this study;[20–22] whether the double mutant folds at concentrations of magnesium greater than 10 mM has not been determined. If it does, it would be of interest to compare the kinetics of compaction and tertiary contact formation of the double mutant and Δ P5abc ribozymes to discern whether this variation results from changes in the ribozyme topology resulting from the deletion. Taken together, the results of Figures 3 and 4 connect P4-P6 formation to a large-scale change in the molecular R_g, and they show that the folding of the P4-P6 domain is a precondition for further folding and justify designation of this domain as the folding scaffold of the *Tetrahymena* ribozyme.[7,8,23]

Since the data for Figure 3 show that no further compaction occurs after formation of the P4-P6 scaffold, it follows that neither subsequent core nor peripheral contact formation contribute to compaction under the low-salt experimental conditions. The absence of a connection between compaction and structuring of the peripheral helices is underscored dramatically by the SAXS data on the triple mutant. With all the long-range contacts linking the peripheral helices disabled, the molecular compaction is as complete as in the wild-type (Figure 2(b)). We conclude from these data that the peripheral helices associate with the core by tertiary interactions distinct from those connecting the ring. Thus, the peripheral ″ring″ contacts play little to no role in mediating compaction but rather serve to rigidify the folded structure. This view of the peripheral helices implies that the outer long-range contacts stabilize the folded RNA rather than play a role in guiding folding.

A lingering ambiguity was that the changes in local solvent accessibility within P4-P6 reporting domain formation lagged global compaction under the conditions of lower background salt (Figure 4). That this result is due to a slight mismatch in experimental conditions and the strong dependence of folding on ionic strength[12,16] was shown by the second series of coordinated SAXS and footprinting studies conducted at a precisely matched higher background monovalent salt (Figure 6). Under these conditions there is remarkable agreement between the timescales of global compaction and formation of the tertiary interactions that stabilize the P4-P6 domain (Figure 7(a)).

However, this difference in background ionic strength also changed the folding landscape. The tertiary interactions present in the RNA at the end of the second compaction phase consist of more than just the P4-P6 domain. Formation of a tertiary contact linking peripheral helices and a tertiary contact structuring the catalytic core are now coincident with the second compaction transition (Figure 7(b) and (c)). Other differences are that regions of the ribozyme that form in concert at lower ionic strength,[8] such as the periphery or the core, are now heterogeneous; the temporal hierarchy P4-P6 > periphery > core observed at very low ionic strength is no longer followed. For example, among the long-range contacts that link the periphery, P14 forms in concert with structuring of the P4-P6 domain and more slowly than P13, which is present at the earliest time sampled (Figure 6(g)). Thus, the second global transition initiates from an ensemble of molecules within which a peripheral long-range contact is already formed.

The above discussions connect tertiary contact formation with the global compactions from 55 Å to 45 Å and from 60 Å to 50 Å in the low-salt and high-salt backgrounds, respectively (Figure 5). However, tertiary contacts also can form independently of significant molecular compaction. This behavior is seen most clearly in progress curves obtained in the low-salt background. The catalytic core of the wild-type molecule begins to fold into its native conformation well after the majority of compaction is complete, with an R_g that is nearly that of the native state (Figure 3(d) and (e)). This relationship is consistent with the conclusion that resolution of the misfolded catalytic core is topologically inhibited by the tight embrace of the linked peripheral helices.[1,24]

The relationship between compaction and catalytic core tertiary structure formation is not as clearcut when Mg^{2+}-mediated folding is carried out at higher ionic strength (Figures 6 and 7). In this case, formation of the tertiary contacts that define the native structure occur during three distinct regions of compaction. (1) The core ·OH protection 265–267 is coincident with the second compaction transition (Figure 7(b)). (2) Nucleotides 279–282 become protected without change in R_g within the 50 Å intermediate that is not present during low-salt folding (Figure 6). (3) The J8/7 region remains minimally structured over the 1 min that the reaction was monitored in these experiments (Figure 6(e)). The J8/7 region is among the slowest, if not the slowest, tertiary contact to form at all the experimental conditions that have been analyzed (I.S. and M.B., unpublished results).[8,12,14] Its folding is thus likely to be the rate-limiting step in the acquisition of catalytic activity. If true, the very different patterns of compaction and tertiary contact formation observed as conditions are varied indicate that the *Tetrahymena* ribozyme can follow very different pathways to its catalytically active structure. We expect this diversity in dominant folding pathways will continue to be seen as global and local measures are monitored concordantly during the folding of other RNA molecules whose biological activity requires that they form unique compact structures.

Conclusion

Concordant measures of global compaction and local changes in solvent accessibility provide a detailed portrait of the time-dependent relationship between compaction and tertiary contact formation during the Mg^{2+}-mediated folding of a large RNA. The earliest monitored events, 1 ms after the initiation of folding, are dominated by the rapid formation of a compact and predominantly non-specifically collapsed ensemble of structures containing, at most, a small fraction of native and/or non-native tertiary contacts. The extent of compaction of this intermediate varies when folding is initiated in different backgrounds of ionic strength; these differences are linked to the transient formation of non-native interactions. The majority of tertiary contacts form from within this compact ensemble. Evidence for the role of the P4-P6 domain as the scaffold for folding of the *Tetrahymena* ribozyme is clearly evident in both the global and local progress curves. For this complex molecule, the scaffold plays a dual role: in addition to establishing a local folding nucleus, it organizes distant elements, bringing them into close proximity for stabilization *via* tertiary contacts. The final stages of folding, in which the contacts that are critical for catalysis and thus biological function are formed, occur within a highly compact ensemble, under some experimental conditions without any further reduction in the molecular envelope. For the *Tetrahymena* ribozyme, the relationship between tertiary contact formation and compaction defies a unique description; folding of this large RNA is a subtly tuned process that ultimately results in biological function.

Materials and Methods

RNA preparation

Wild-type and four mutants of the L-21 ScaI ribozyme from *T. thermophila*[25] were prepared by *in vitro* transcription as described.[26] The double mutant ribozyme bears mutations of the A-rich bulge (AAUAAG (183–188) to UUUUUU) and the tetraloop receptor (UAAG (224–227) to AUA) destabilizing the major interhelix tertiary contacts within the P4-P6 domain.[27] The triple mutant bears mutations of L2 (GGCAUGCACCU (39–49) to CUUCGGU), L9 (AAU (324–326) to C), and L9.1 (GAUGCAAC (346-353) to CUUCGG) destabilizing the major tertiary contacts between the peripheral helices. The quintuple mutant carries both sets of mutations.

RNA utilized for the ·OH footprinting experiments was radiolabeled at either the 5′ end with [γ-^{32}P]ATP by phosphatase treatment followed by kinasing,[25] or the 3′ end with [α-^{32}P]dCTP by Klenow polymerase using a modified published protocol.[12,28] The radiolabeled RNA was gel-purified, precipitated and resuspended in the assay buffer.[27] RNA used in the SAXS experiments was purified by passage through a Qiagen RNeasy column following the manufacturer's instructions.

Time-resolved SAXS data acquisition

A microfabricated continuous-flow mixer was used to acquire SAXS data on the most rapid timescales of $<$160 ms.[5] RNA was added to buffer containing 50 mM Na–Mops (3-(*N*-morpholino)propanesulfonic acid) at pH 7.0, or 10 mM potassium Mops, 100 mM KCl at pH 7.0 as indicated in the text. The final RNA concentration was adjusted to 4 mg/mp. The RNA was denatured by heating to 95 °C for 1 min and then allowed to cool to room temperature. This solution flows into one port of the continuous-flow mixer against a solution of equivalent buffer containing 10 mM $MgCl_2$ flowing into two orthogonal ports. The flow of these two channels focuses the solution of RNA into a thin jet. Folding is triggered by the rapid diffusion of Mg^{2+} into the jet of RNA. The flow-speed of the fluid was controlled with a programmable syringe pump (Harvard Instruments). By combining data obtained using fast[5] and slow flow-rates, timescales ranging from 1 ms to 160 ms are accessible with this apparatus. SAXS progress curves were obtained by positioning the X-ray beam at a fixed location along the outlet channel of the continuous-flow mixer. Each position corresponds to an elapsed time after mixing. The time-courses shown in Figures 2 and 5 were generated by taking data at multiple positions along the flow cell. All of the SAXS experiments were carried out at 25 °C. These studies used attenuated "pink beam" generated at the 8-ID-I beamline at the Advanced Photon Source.[29] An X-ray flux of 3×10^{10} photons/s was measured in the 10 μm×40 μm beam. Scattering profiles were collected with a Princeton Instruments X-ray detector located at the end of an evacuated 50 cm long beampipe.

A BioLogic SFM stopped-flow mixer was used to access folding times longer than 160 ms (Bio-Logic Science Instruments, France). Folding buffer containing 32 mM Mg^{2+} was mixed with RNA in an appropriate ratio to reach the desired final concentration of 2 mg/ml of RNA and 10 mM free Mg^{2+}. The observation cuvettes were optimized for SAXS measurements. Ultra-thin silicon nitride membranes that were fabricated at the Cornell NanoScale Science and Technology Facility were employed as X-ray windows. These experiments used 10 keV X-rays generated at the Cornell High Energy Synchrotron Source's G-1 station (beam flux 10^{11} photon/s into a 1 mm^2 spot). This apparatus was capable of accessing timescales ranging from 0.1 s to 300 s. Scattering profiles were collected with a MedOptics CCD detector positioned at the end of an evacuated 50 cm long beampipe.

Time-resolved SAXS data analysis

Guinier analysis of the data[30] was employed to extract the radius of gyration (R_g) of the RNA from scattering profiles acquired at numerous locations along the outlet channel that correspond to different times after the initiation of folding. The acquisition of good-quality scattering signals at the lowest scattering angles enables an R_g analysis. The Guinier approximation is valid in the range $0.0181\ \text{Å}^{-1} < q < 0.0317\ \text{Å}^{-1}$, where $q=4\pi\sin\theta/\lambda$, 2θ is the scattering angle, and $\lambda=1.64$ Å is the X-ray wavelength. To extract R_g, the natural logarithm of the measured scattered intensity is plotted as a function of q^2. In this small angle limit, the slope of the straight line through these points is directly proportional to R_g^2. MATLAB software was used for all image processing and data analysis. In previous studies,[5,6] where data at the smallest scattering angles were obscured, two-state projections based on singular-value decomposition of the data was employed. There is good agreement between the time constants obtained with both methods. However the Guinier analysis used here provides an additional quantitative parameter, the overall size of the molecule.

Time-resolved synchrotron ·OH footprinting

Radiolabeled RNA was suspended in buffer containing 0.1 mM EDTA and 10 mM sodium cacodylate (pH 7.0) for the low-salt experiments. The concentration of Na^+ in the buffer for footprinting at the low-salt condition was matched to the Na^+ concentration of the Na-Mops buffer used for the first set of trSAXS experiments. This CE-SAXS buffer contains 19 mM Na^+ and 23 mM sodium cacodylate. For the experiments conducted at 100 mM KCl, the [^{32}P]RNA was diluted in buffer containing 10 mM potassium cacodylate (pH 7.0), 0.1 mM EDTA (CE-K) and stored at −70 °C. The [^{32}P]RNA was kept frozen until just prior to the set-up of a kinetics analysis.

Time-resolved ·OH footprinting experiments were performed at Beamline X-28C at the National Synchrotron Light Source, Brookhaven National Laboratory as described.[12,14,29,31,32] A new X-ray exposure chamber allowed irradiation times of 7–12 ms to be used in these studies (M. Sullivan, J. Toomey, S. Gupta, M. R. Chance & M.B., unpublished results). The earliest reaction time sampled was 15 ms.

The ionic strength of the [^{32}P]RNA solution was adjusted to either the CE-SAXS or CE-K plus 100 mM KCl buffer. The solution was denatured by heating to 95 °C for 1 min, then cooled slowly and incubated at 25 °C prior to initiating the kinetics experiment. Folding reactions were initiated in the rapid mixer by mixing 20 μl of sample with an equal volume of initial buffer plus 20 mM $MgCl_2$ at 25 °C. The expelled RNA samples were precipitated with ethanol. The RNA products following ·OH degradation were separated by denaturing polyacrylamide gel electrophoresis. Dried gels were imaged by exposure of a storage phosphor screen that was scanned by a Molecular Dynamics™ Storm™ imager.

The ·OH reactivity of groups of nucleotides comprising tertiary contacts that changed as a result of RNA folding were quantified by "block" analysis using ImageQuant™ (Molecular Dynamics™).[8,11,12,14,33] The data sets were scaled individually to fractional saturation, $\bar{Y}$, by:

$$f_i = L + (U - L)\bar{Y} \tag{1}$$

where f denotes the integrated density of the bands, and L and U represent the lower and upper limits to the transition, respectively. The lower limit L was determined from RNA in initial buffer and the upper limit U was determined from samples folded for 1 h at 25 °C under the ionic condition of experiments in 10 mM $MgCl_2$.The kinetics progress curves were fit using non-linear, least-square analysis in Origin® 6.1 (OriginLab®) to single to triple-exponentials according to the equation:

$$\bar{Y} = 1 - \sum_{i=1} \alpha_i \exp(-k_i t) \tag{2}$$

where α_i and k_i are the amplitude and rate constant, respectively, of the ith kinetic phase. The rate constant for the burst phase was fixed at 50 s^{-1} so that error estimates on the burst amplitude could be obtained. The value of 50 s^{-1} is the minimal rate consistent with the acquisition of the first data point. The lower and upper bounds calculated by the Origin software at the 65% confidence interval (one standard deviation) are reported.

Acknowledgements

This work was supported by grant P01-GM066275 from the National Institute of General Medical Sciences. Use of the Advanced Photon Source was supported by the U.S. Department of Energy, Office of Science, Office of Basic Energy Sciences, under contract no. W-31-109-Eng-38. We acknowledge additional support from NASA under contract number NAG8-1778 (to L.P.), and from the National Science Foundation through grant MCB-0347220 (to L.P.) and the Cornell Nanobiotechnology Center. This work is also based upon research conducted at the Cornell High Energy Synchrotron Source (CHESS), which is supported by the National Science Foundation and the National Institutes of Health/National Institute of General Medical Sciences under award DMR-0225180. The X-ray footprinting studies were conducted at beamline X-28C of the National Synchrotron Light Source supported by grant P41-EB0001979 from the National Institute of Biomedical Imaging and Bioengineering. Fabrication of the SAXS mixing devices was conducted in the Cornell Nanoscale Science and Technology Facility that is supported by the NSF, Cornell University and industrial affiliates. We thank Sayan Gupta for his support of beamline X-28C operations, Simon Mochrie for the generous loan of a stopped-flow mixer, Alec Sandy and Suresh Narayanan for their assistance at beamline 8-IDI at the APS, and Arthur Woll and Ernie Fontes for assistance at the CHESS G-1 beamline. We thank Rhiju Das and Dan Herschlag for helpful discussions.

References

1. Treiber, D. K. & Williamson, J. R. (1999). Exposing the kinetic traps in RNA folding. *Curr. Opin. Struct. Biol.* **9**, 339–345.
2. Thirumalai, D., Lee, N., Woodson, S. A. & Klimov, D. K. (2001). Early events in RNA folding. *Annu. Rev. Phys. Chem.* **52**, 751–762.
3. Sosnick, T. R. & Pan, T. (2003). RNA folding: models and perspectives. *Curr. Opin. Struct. Biol.* **13**, 309–316.
4. Doniach, S. (2001). Changes in biomolecular conformation seen by small angle X-ray scattering. *Chem. Rev.* **101**, 1763–1778.
5. Russell, R., Millettt, I. S., Tate, M. W., Kwok, L. W., Nakatani, B., Gruner, S. M. *et al*. (2002). Rapid compaction during RNA folding. *Proc. Natl Acad. Sci. USA*, **99**, 4266–4271.
6. Das, R., Kwok, L. W., Millett, I. S., Bai, Y., Mills, T. T., Jacob, J. *et al*. (2003). The fastest global events in RNA folding: electrostatic relaxation and tertiary collapse of the *Tetrahymena* ribozyme. *J. Mol. Biol.* **332**, 311–319.
7. Zarrinkar, P. P. & Williamson, J. R. (1994). Kinetic intermediates in RNA folding. *Science*, **265**, 918–924.
8. Sclavi, B., Sullivan, M., Chance, M. R., Brenowitz, M. & Woodson, S. A. (1998). RNA folding at millisecond intervals by synchrotron hydroxyl radical footprinting. *Science*, **279**, 1940–1943.
9. Latham, J. A. & Cech, T. R. (1989). Defining the inside and outside of a catalytic RNA molecule. *Science*, **245**, 276–282.
10. Takamoto, K., He, Q., Morris, S., Chance, M. R. & Brenowitz, M. (2002). Monovalent cations mediate formation of native tertiary structure of the *Tetrahymena* thermophila ribozyme. *Nature Struct. Biol.* **9**, 928–933.
11. Sclavi, B., Woodson, S., Sullivan, M., Chance, M. & Brenowitz, M. (1998). Following the folding of RNA with time-resolved synchrotron X-ray footprinting. *Methods Enzymol.* **295**, 379–402.
12. Shcherbakova, I., Gupta, S., Chance, M. R. & Brenowitz, M. (2004). Monovalent ion-mediated folding of the *Tetrahymena* thermophila ribozyme. *J. Mol. Biol.* **342**, 1431–1442.
13. Russell, R., Millett, I. S., Doniach, S. & Herschlag, D. (2000). Small angle X-ray scattering reveals a compact intermediate in RNA folding. *Nature Struct. Biol.* **7**, 367–370.
14. Uchida, T., Takamoto, K., He, Q., Chance, M. R. & Brenowitz, M. (2003). Multiple monovalent ion-dependent pathways for the folding of the L-21 *Tetrahymena* thermophila ribozyme. *J. Mol. Biol.* **328**, 463–478.
15. Silverman, S. K., Deras, M. L., Woodson, S. A., Scaringe, S. A. & Cech, T. R. (2000). Multiple folding pathways for the P4-P6 RNA domain. *Biochemistry*, **39**, 12465–71245.
16. Deras, M. L., Brenowitz, M., Ralston, C. Y., Chance, M. R. & Woodson, S. A. (2000). Folding mechanism of the *Tetrahymena* ribozyme P4-P6 domain. *Biochemistry*, **39**, 10975–10985.
17. Russell, R., Zhuang, X., Babcock, H. P., Millett, I. S., Doniach, S., Chu, S. & Herschlag, D. (2002). Channels in the folding landscape of a structured RNA. *Proc. Natl Acad. Sci. USA*, **99**, 155–160.
18. Zheng, M. X., Wu, M. & Tinoco, I. (2001). Formation of a GNRA tetraloop in P5abc can disrupt an interdomain interaction in the *Tetrahymena* group I ribozyme. *Proc. Natl Acad. Sci. USA*, **98**, 3695–3700.
19. Joyce, G. F., Vanderhorst, G. & Inoue, T. (1989). Catalytic activity is retained in the *Tetrahymena* group-I intron despite removal of the large extension of element P5. *Nucl. Acids Res.* **17**, 7879–7889.
20. Doherty, E. A., Herschlag, D. & Doudna, J. A. (1999). Assembly of an exceptionally stable RNA tertiary

interface in a group I ribozyme. *Biochemistry*, **38**, 2982–2990.

21. Engelhardt, M. A., Doherty, E. A., Knitt, D. S., Doudna, J. A. & Herschlag, D. (2000). The P5abc peripheral element facilitates preorganization of the *Tetrahymena* group I ribozyme for catalysis. *Biochemistry*, **39**, 2639–2651.
22. Johnson, T. H., Tijerina, P., Chadee, A. B., Herschlag, D. & Russell, R. (2005). Structural specificity conferred by a group I RNA peripheral element. *Proc. Natl Acad. Sci. USA*, **102**, 10176–10181.
23. Downs, W. D. & Cech, T. R. (1996). Kinetic pathway for folding of the *Tetrahymena* ribozyme revealed by three UV-inducible crosslinks. *RNA*, **2**, 718–732.
24. Pan, J. & Woodson, S. A. (1999). The effect of long-range loop-loop interactions on folding of the *Tetrahymena* self-splicing RNA. *J. Mol. Biol.* **294**, 955–965.
25. Zaug, A. J., Grosshans, C. A. & Cech, T. R. (1988). Sequence-specific endoribonuclease activity of the *Tetrahymena* ribozyme-enhanced cleavage of certain oligonucleotide substrates that form mismatched ribozyme substrate complexes. *Biochemistry*, **27**, 8924–8931.
26. Russell, R. & Herschlag, D. (1999). New pathways in folding of the *Tetrahymena* group I RNA enzyme. *J. Mol. Biol.* **291**, 1155–1167.
27. Takamoto, K., Das, R., He, Q., Doniach, S., Brenowitz, M., Herschlag, D. & Chance, M. R. (2004). Principles of RNA compaction: Insights from the equilibrium folding pathway of the P4-P6 RNA domain in monovalent cations. *J. Mol. Biol.* **343**, 1195–1206.
28. Huang, Z. & Szostak, J. W. (1996). A simple method for $3'$-labeling of RNA. *Nucl. Acids Res.* **24**, 4360–4361.
29. Sandy, A. R., Lurio, L. B., Mochrie, S. G. J., Malik, A., Stephenson, G. B., Pelletier, J. F. & Sutton, M. (1999). Design and characterization of an undulator beamline optimized for small-angle coherent X-ray scattering at the Advanced Photon Source. *J. Synchrot. Radiat.* **6**, 1174–1184.
30. Glatter, O. (1982). *Small Angle X-ray Scattering*, Academic Press, London UK.
31. Ralston, C. Y., Sclavi, B., Sullivan, M., Deras, M. L., Woodson, S. A., Chance, M. R. & Brenowitz, M. (2000). RNA-ligand interactions, *Methods Enzymol.* **317**, 353–368.
32. Dhavan, G., Chance, M. & Brenowitz, M. (2003). *Kinetics Analysis of DNA-Protein Interactions by Time-resolved Synchrotron X-ray Footprinting*, IRL Press at Oxford University Press, Oxford, UK.
33. Brenowitz, M., Senear, D. F., Shea, M. A. & Ackers, G. K. (1986). Quantitative DNAse footprint titration-a method for studying protein-DNA interactions. *Methods Enzymol.* **130**, 132–181.

Edited by D. E. Draper

(Received 25 August 2005; received in revised form 21 October 2005; accepted 25 October 2005)